

SEISMIC RESPONSE OF PILE-SUPPORTED STRUCTURE CONSIDERING NONLINEARITY OF SUPERSTRUCTURE AND PILE, AND LIQUEFACTION OF SURROUNDING GROUND

Osamu KURIMOTO Takeshi FUJIMORI Yuzuru YASUI

*Technical Research Institute, Obayashi Corporation
4-640, Shimokiyoto, Kiyose-shi, Tokyo 204-0011, JAPAN
E-mail : kurimoto@tri.obayashi.co.jp*

ABSTRACT

Recent earthquake disasters have revealed the importance of countermeasures against soil liquefaction in seismic design. In particular, the 1995 Hyogoken Nanbu earthquake caused several types of severe damages to pile foundations. This paper describes an analysis method for soil liquefaction using simple parameters such as SPT-*N* values and seismic response analyses for the pile-supported structure to consider soil-structure interaction effects and soil non-linearity using a modified Penzien model. It is important to find a way to determine the region of surrounding soil whose behavior is identical to that of piles. This paper adopts the thin layer element method to systematically determine the volume of the surrounding soil. The responses of pile-supported structure are similar, whether soil liquefaction and nonlinearity of pile are considered or not. However, the bending moments of pile become large as to soil liquefaction, and small as to nonlinearity of pile.

Keywords Pile Supported Structure Modified Penzien model Effective Soil Column
Liquefaction of Soil Nonlinear Moment-Curvature Relationship

1. Introduction

Recent earthquake disasters have revealed the importance of countermeasures against soil liquefaction in seismic design. In particular, even the backfill soil with gravel that does not supposed to be liquefied has liquefied at the 1995 Hyogoken Nanbu earthquake (Kobe earthquake). This new type of liquefaction gave great impact in seismic design. Many researchers have elucidated the behavior of soil liquefaction and developed the simulation method. As a result, some computer programs can evaluate the behavior. However, the laboratory tests must be performed to determine many liquefaction parameters that these computer programs require. This paper describes simplified method to analyze the dynamic characteristics of soil liquefaction. A proposed method needs only few parameters that are decided by the usual boring investigation. Simulation analysis for Kobe Port Island vertical array records of Kobe earthquake was performed to verify the validity of analysis method, and the analysis results coincided well with the observed one. In order to estimate accurately the dynamic behavior of pile-supported structure, not only the super structure but also piles and soil nonlinearity must be considered. The Penzien model has the advantages in practical use to investigate the nonlinear behavior of pile-supported structure. However, the evaluation of soil spring between pile and free field soil column is important because the seismic response is affected by

the stiffness and damping of soil spring. In recent years, the thin layer element method has been used to determine the impedance matrix of pile groups and reduced to the axial soil spring between pile and free field soil column, and the shear spring in near field soil column in accordance with pile [Miyamoto et al. (1997)].

The modified Penzien model is physically comprehensive because the effective mass is treated as to be substantial. However, there still exists some problem that the area of effective mass affects the seismic response. This paper presents a rational method to determine the effective mass, and discusses the effect of nonlinear seismic response of soil-pile structure system including soil liquefaction.

2. Simplified evaluation of parameters for effective stress analysis

2.1 Liquefaction resistance

The cyclic stress ratio that is the liquefaction resistance may be expressed in terms of number of cycles required to cause liquefaction.

$$\frac{t}{s_0} = R_{20} \left(\frac{N}{20} \right)^C \dots\dots\dots(1)$$

where s_0 means the initial effective confining stress, R_{20} is the stress ratio produced a condition of

liquefaction without cyclic mobility by 20 uniform stress cycles and C means the parameter between cyclic stress ratio and number of cycles. C takes -0.2 through -0.3, and usually takes -0.25. Fig.1 shows the liquefaction resistance normalized by R_{20} with $C=-0.20$, -0.25 and -0.30. The recommendations for design of building foundations(AIJ 1988) provides the liquefaction resistance by

$$\frac{t_l}{s_z} = aC_f \left[\frac{16\sqrt{N_1 + \Delta N_f}}{100} + \left(\frac{16\sqrt{N_1 + \Delta N_f}}{C_s} \right)^n \right] \dots\dots\dots (2)$$

$$N_1 = C_N N, \quad C_N = \sqrt{10/s_z}$$

$$\Delta N_f = \begin{cases} 0 & : FC \leq 5 \\ 1.2FC - 6 & : 5 \leq FC \leq 10 \\ 0.2FC + 4 & : 10 \leq FC \leq 20 \\ 0.1FC + 6 & : 20 \leq FC \end{cases}$$

where N_1 is the normalized SPT N_1 -value at $s_0=1\text{kgf/cm}^2$. ΔN_f is a constant and can be considered as a correction term for taking into account the effect of fines content. Note that the normalized SPT N_1 -value may be estimated to be small values when the effective vertical stress is small.

Equation (2) expresses the liquefaction resistance to effective vertical stress and R_{20} in equation (1) expresses the liquefaction resistance to the effective mean confining stress. Therefore R_{20} should be corrected as

$$R_{20} = \frac{1+2K_0}{3} \frac{t_l}{s_z}$$

in which K_0 is assumed to be 0.5

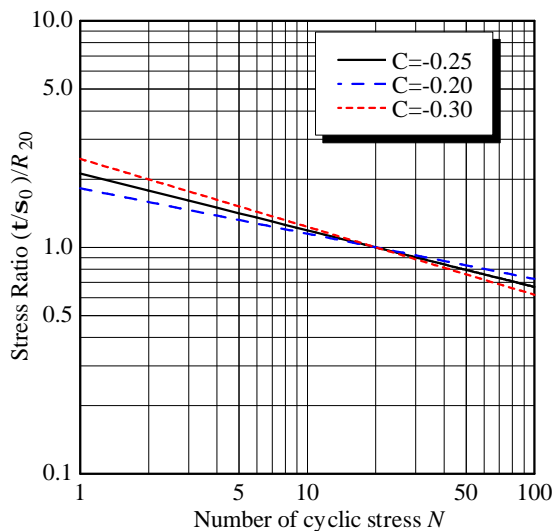


Fig. 1 Relationships between Cyclic Stress Ratio and Number of Cycles Required to Cause Liquefaction

2.2 Buildup of excess pore water pressure

Seed et al. (1976) obtained the following relationship between the excess pore water pressure and shear stress using undrained shear test for the saturated sand.

$$\frac{u_g}{s_{0i}} = \frac{2}{p} \sin^{-1} \left(\frac{N}{N_{liq}} \right)^{\frac{1}{2a}} \dots\dots\dots (3)$$

where u_g is the excess pore water pressure, N/N_{liq} is the ratio of equivalent uniform stress cycles required to cause liquefaction. a means a function of soil properties and test conditions, and usually $a=0.7$. Fig.2 shows the change of the increase of excess pore water pressure against a that varies 0.5, 0.7 and 0.9.

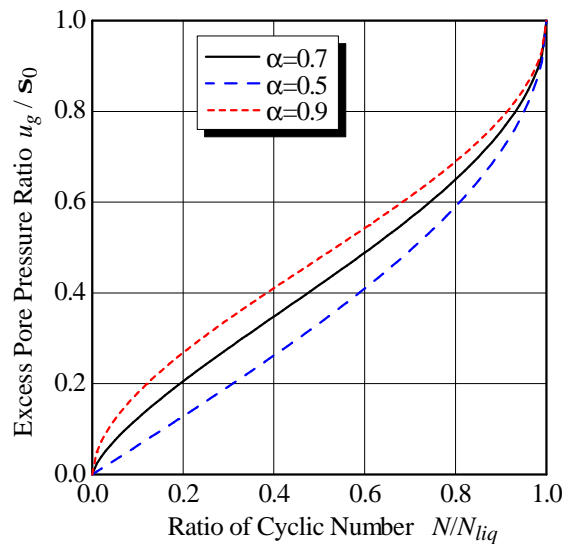


Fig.2 Rate of Pore Water Pressure Buildup in Cyclic Simple Shear Tests

Equation (3) shall be modified so that the build up of excess pore water pressure can be estimated in case of shear stress generated by the irregular excitation as seismic response. The fatigue damage concept is adopted as similar to Shamoto et al. (1992).

The modified Ramberg-Osgood model and the masing rule are adopted as the skeleton curve and the unloading curve, respectively, for the nonlinear relationship between shear stress and shear strain of soil.

[Skeleton Curve]

$$g = \frac{1}{G} t \left(1 + a |t|^b \right) \dots\dots\dots (4)$$

[Unloading Curve]

$$\frac{g - g_a}{2} = \frac{1}{G} \frac{t - t_a}{2} \left(1 + a \left| \frac{t - t_a}{2} \right|^b \right) \dots\dots\dots (5)$$

$$\left. \begin{aligned} \mathbf{b} &= \frac{2\mathbf{p} h_{\max}}{2-\mathbf{p} h_{\max}}, \mathbf{a} = \left(\frac{2}{G \cdot \mathbf{g}_r} \right)^{\mathbf{b}} \\ G &= G_0 \left(\frac{\mathbf{s}'}{\mathbf{s}'_0} \right)^m, \mathbf{g}_r = \mathbf{g}_{r0} \left(\frac{\mathbf{s}'}{\mathbf{s}'_0} \right)^m \end{aligned} \right\} \dots\dots\dots (6)$$

where G_0 is the initial shear modulus, h_{\max} is the maximum damping factor, and \mathbf{g}_{r0} is the initial reference shear strain at which the shear modulus reduce to a half of the initial shear modulus. m is a constant that expresses the confining pressure dependency of shear modulus and reference shear strain, and usually 0.5 is adopted as m . \mathbf{s}' is the mean effective confining stress, \mathbf{s}'_0 the initial mean effective confining stress.

The excess pore water pressure at i -th step in time response is estimated by the following equation.

$$\frac{u_{gi}}{s_{0i}} = \frac{2}{\mathbf{p}} \sin^{-1} R_i \frac{1}{2^{\mathbf{a}}} \dots\dots\dots (7)$$

where $R_i = \sum (1/N_i - 1/N_{i-1})$, and N_i is

$$N_i = 0.5 \cdot 20 \left(R_{20} \frac{t_i - t_a}{s_0} \right)^{\frac{1}{C}} = 10 \left(R_{20} \frac{t_i - t_a}{s_0} \right)^{\frac{1}{C}} \dots\dots\dots (8)$$

The point (t_a, \mathbf{g}_a) is the reversed point of hysteresis loop. When the hysteresis loop reverses, set $1/N_{i-1}=0$. R_i expresses the contribution to the increase of pore water pressure when shear stress varies the point A through the point B or the point B through the point C in Fig. 3. The basic concept of equations (7) and (8) is that Fig. 1 is considered to be the fatigue damage similar to metal material. When the stress ratio $(t_i - t_a)/s_0$ of 1 cycle is applied, the contribution to the excess pore water pressure is expressed as $1/N_i$. N_i can be obtained from equation (8).

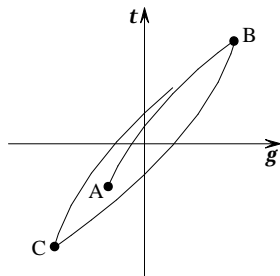


Fig. 3 Hysteresis Curve in Ramberg-Osgood Model

2.3 Change of excess pore water pressure during cyclic mobility

The cyclic mobility is evaluated as same as YUSAYUSA developed by Ishihara et al. (1980). The

critical state line is defined by Mohr-Coulomb failure criterion ($t = s'_v \tan f_L$) on the shear stress (t) -effective stress (s'_v) plane. The cyclic mobility occurs at the condition $t/s'_v > \tan f_m$. The line on equation $t = s'_v \tan f_m$ is called the phase transformation line. f is the usual internal friction angle, f_L is the internal friction angle ($\tan f_L \approx 1.4 \tan f$) when the effective stress is small, and f_m is the phase transformation angle ($\tan f_m \approx 0.875 \tan f$).

Fig. 4 shows the failure line of Mohr-Coulomb and the phase transformation line, and the effective stress path (1) and (2) as follows.

The path (1) shown in equation (9) expresses that the excess pore water pressure decreases when t/s'_v exceeds $\tan f_m$ and the shear stress still increases.

$$\left(\frac{s'_v}{m} \right)^2 - \left(\frac{t}{m \tan f_L} \right)^2 = 1 \dots\dots\dots (9)$$

where m is a parameter that decides the position of parabola by equation (9) on the shear stress-effective stress plane. m is determined as follows. When the shear stress t_a and effective stress s'_{va} crosses the phase transformation line, the following equation $s'_{va} \tan f_m = t_a$ is formed. Substituting this relationship for equation (9), then leads equation (10).

$$\left(\frac{t_a}{m \tan f_m} \right)^2 - \left(\frac{t_a}{m \tan f_L} \right)^2 = 1 \dots\dots\dots (10)$$

Solving Equation (10) for m leads

$$m = \sqrt{\left\{ \left(\frac{1}{\tan f_m} \right)^2 - \left(\frac{1}{\tan f_L} \right)^2 \right\} t_a} \dots\dots\dots (11)$$

The path (2) expresses that t/s'_v moves the tangent line of parabola and the excess pore water pressure increases when the shear stress decreases

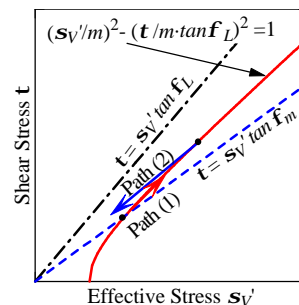


Fig. 4 Effective Stress Path

2.4 Characteristics of liquefaction model

The shear stress-shear strain relationship and stress path of an element subjected to cyclic strain is discussed. Fig. 5 shows the response characteristics comparing the total stress analysis and effective stress analysis. It is found that the excess pore water pressure builds up gradually and required number of cyclic stress for liquefaction in case of the effective stress analysis while the excess pore water pressure generates quickly and the complete liquefaction occurs in case of the total stress analysis. The stress-strain relationship shows the inverse S shape and the cyclic mobility revives soil stiffness when stress path crosses the phase transformation line.

2.5 Simulation analysis for Kobe Port Island vertical array records at the 1995 Hyogoken-Nanbu Earthquake

The backfill soil around the port was caused liquefaction in Kobe earthquake. The valuable observation records at Kobe Port Island including liquefaction phenomenon was obtained. The observation records were simulated by using the above mentioned analytical technique. Analytical conditions and results are described in (1) - (6).

(1) The earthquake observation point is located in the northwest part of Port Island, and is presumed to have generated liquefaction because no countermeasures were done while the surrounding ground of the building was improved.

The soil profile and the depth of installed seismograph are shown in Table 1 reported by Kobe City Development Bureau (1995).

(2) The nonlinear parameters for R-O model of soil material are the reference strain g_0 and maximum damping factor h_{max} . The following values are used because detailed laboratory test data are insufficient.

Depth	Reference Strain	Max. Damping
G.L. 0.0m ~ G.L. -27.0m	$g_0=5 \times 10^{-4}$	$h_{max}=0.2$
G.L. -7.0m ~ G.L. -83.0m	$g_0=1 \times 10^{-3}$	$h_{max}=0.2$

(3) The parameters of liquefaction resistance are determined by SPT-N value, content rate of fine grain size FC and the internal friction angle. FC was assumed to be 10%. SPT-N value is used the average SPT-N value in Table 1. The internal friction angle is determined by Meyerhof's empirical equation $f=0.25N+32.5$.

(4) The Rayleigh damping of 2% for 1st and 2nd predominant frequency is given to be stable in numerical calculation.

(5) The NS component of record which has been observed with GL-83m in Kobe earthquake is used as incidence wave (E+F).

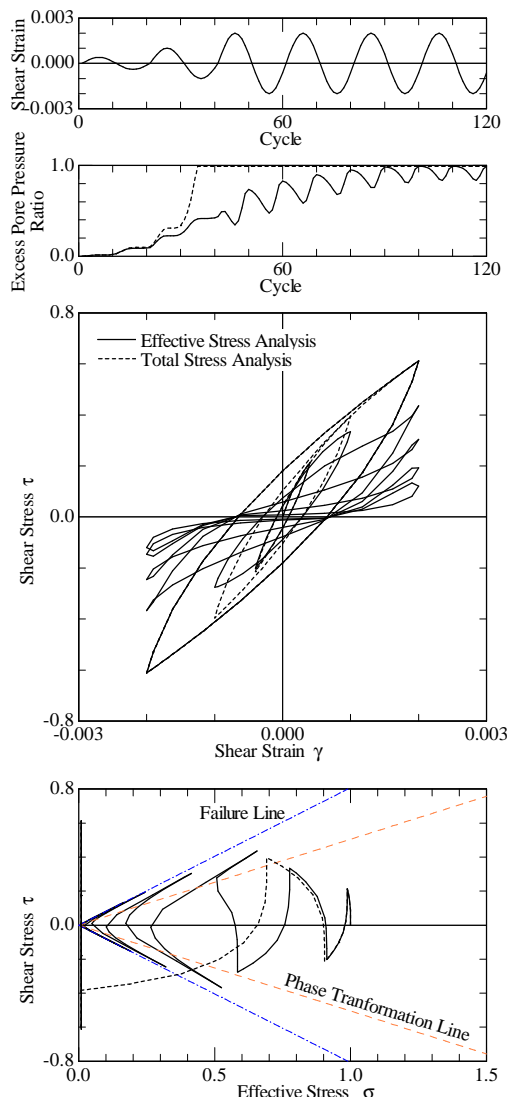


Fig. 5 Response Characteristics of 1 Element Model

Table 1 Soil Properties of Kobe Port Island for Analysis

Acc. G.L. 0m	depth G.L. (m)	soil profile	V _p (m/s)	V _s (m/s)	ave. SPT-N	density (tf/m ³)	
-16m	0.0~2.0	sandy gravel	backfill	260	170	5.2	1.80
	2.0~5.0	sandy gravel		330	170	5.2	1.80
	5.0~12.6	sandy gravel		780	210	6.5	1.80
	12.6~19.0	sand with gravel		1480	210	6.5	1.80
-32m	19.0~27.0	clay	alluvium	1180	180	3.5	1.50
	27.0~33.0	sand	alluvium	1330	245	13.5	1.50
	33.0~50.0	sand with gravel	dilluvium	1530	305	36.5	1.85
-83m	50.0~61.0	sand	dilluvium	1610	350	61.9	1.85
	61.0~79.0	clay	dilluvium	1610	303	11.7	1.85
	79.0~85.0	sand with gravel	dilluvium	2000	320	68.0	1.85

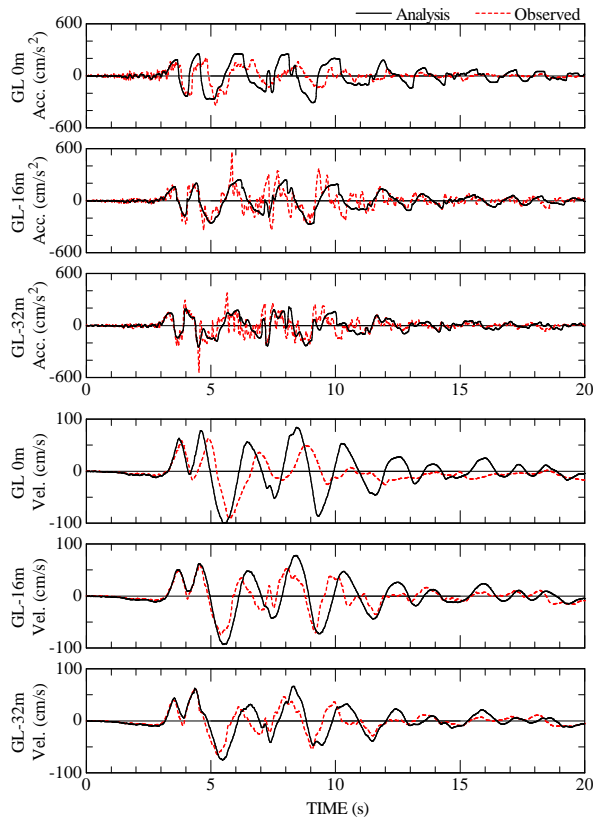


Fig. 6 Nonlinear Soil Response of Port Island Vertical Array

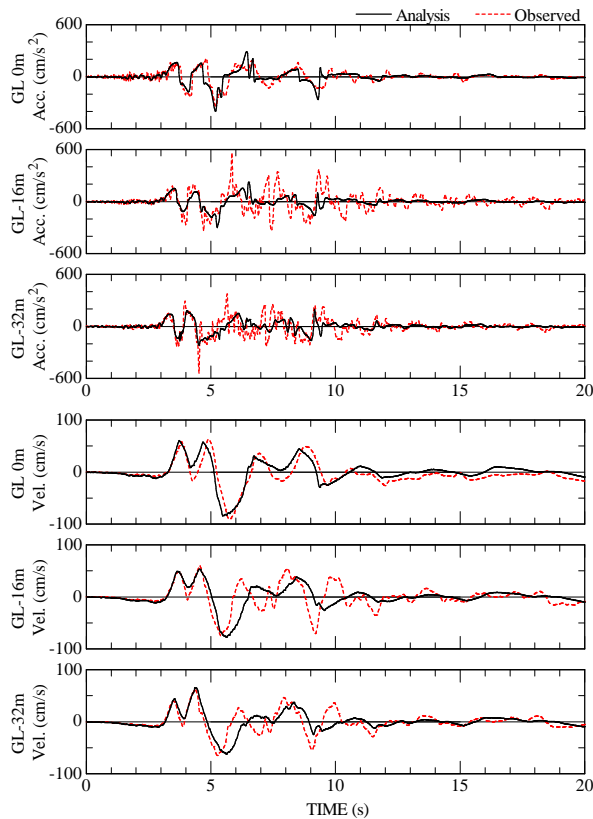


Fig. 7 Effective Stress Analysis of Port Island Vertical Array

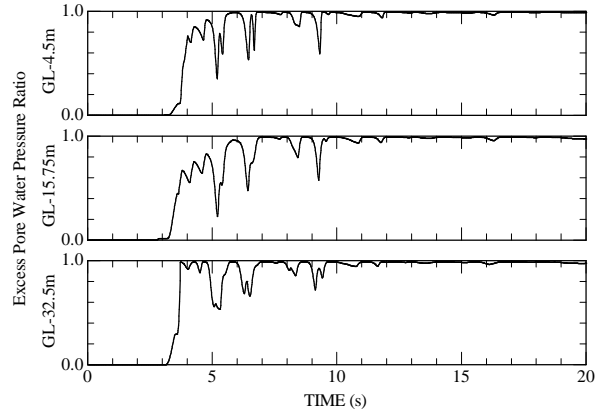


Fig. 8 Time History of Excess Pore Water Pressure Ratio

(6) Fig. 6 shows the comparison of the response when only nonlinearity of soil using R-O model is first considered. The velocity time history of the observation is integrated from the acceleration. The analysis results of the first part of acceleration and velocity correspond to those of observed well. The envelop shapes of waves also coincide well at the position of G.L.-32m. However, the amplitudes of analysis results at G.L.0m overestimate in the latter half part of waves because the upward wave propagation is lost by liquefaction in the observation record.

Next, the result of the effective stress analysis by which the cyclic mobility is considered is shown in Fig. 7. The tendency to the observation record at G.L.0m agrees well. Especially, the velocity response shows very good correspondence. On the other hand, there is often no correspondence compared with the case where liquefaction is not considered at G.L.-32m. Fig. 8 shows the time history of excess pore water pressure built up. The excess pore water pressures rise rapidly around 3.5 seconds in the each level. Those reaches the initial liquefaction at about 4 seconds, and has almost become the complete liquefaction at 10 seconds though the decrease and increase of excess pore water pressure are repeated by cyclic mobility.

3. Seismic response analysis considering nonlinearities of soil-pile-structure system

3.1 Determination of effective soil column in modified Penzien model

First of all, the thin layer element method using the ring excitation solution leads the *frequency dependent* complex impedance matrix of pile groups [Takano et al. (1994)] when the displacement mode is assumed, the impedance matrix reduces and separates to the axial and shear spring which are still *frequency dependent*. Next, those springs approximate to be *frequency independent* constant spring, dashpot and additional mass. An equivalent soil column with this shear spring corresponds to the soil in accordance

with pile. The effective soil column of the modified Penzien model can be determined by this procedure.

3.2 Analytical model

The 6 stories and 15 stories pile supported structures are assumed to be constructed at Kobe Port Island [Fujimori et al. (1998)]. The superstructure is substituted for one mass with equivalent height and equivalent mass. The level of underground floor bottom is G.L. -6m, and the pile head and the underground floor are assumed to be a rigid joint. 36 reinforced concrete piles with a diameter 1.3m in 6 stories structure and a diameter 1.9m in 15 stories structure are supported to the dilluvium of G.L. -51m. The superstructure is modeled by the shear spring with trilinear force-displacement relationships. The pile is modeled by the beam element with trilinear moment-curvature relationships. The nonlinear characteristics are derived from the fiber model. The shear force(Q)-displacement(d) relationship of pile is assumed to be linear. The axial spring that connects the effective mass and free field soil is also assumed to be linear. The shear stress-strain relationship is considered the liquefaction including cyclic mobility.

The input motion for the soil-pile-structure model as shown in Fig. 9 is defined at G.L. -51m using observation record of Kobe Port Island of Kobe earthquake [Fujimori et al. (1998)].

3.3 Results and discussion

The equivalent area of effective soil column is obtained by equation (12), and is shown in Fig. 10.

$$\left. \begin{aligned} A_K &= \sum A_{Ki} \ell_i / \sum \ell_i, A_{Ki} = K_{bi} \ell_i / G_i \\ A_M &= \sum A_{Mi} \ell_i / \sum \ell_i, A_{Mi} = M_{ai} / \ell_i r_i \end{aligned} \right\} \dots\dots\dots (12)$$

in which A_K is the equivalent area of the effective soil column based on the averaging shear spring. A_M is also the equivalent area of the effective soil column but based on the averaging additional mass. K_{bi} is the shear spring of i -th layer obtained from the thin layer element method, ℓ_i , G_i and r_i are the thickness, shear modulus and mass density of i -th layer, respectively. Fig. 10 indicates that the equivalent area of effective soil column with the shear spring by the thin layer element method would be small rather than the area of basement.

The seismic response analyses for soil-pile-structure system were performed. The analysis cases were focused on the soil liquefaction and pile nonlinearity as shown in Table 2.

Figs. 11 and 12 show the response time histories, velocity response spectra and maximum values. The maximum values of acceleration and displacement considering soil liquefaction become larger than those

not considering soil liquefaction. The velocity response spectra are the different whether soil liquefaction is considered or not. On the other hand, the pile nonlinearity does not affect on the maximum values and response spectra. These are common tendency in the responses of 6 and 15 stories structure models.

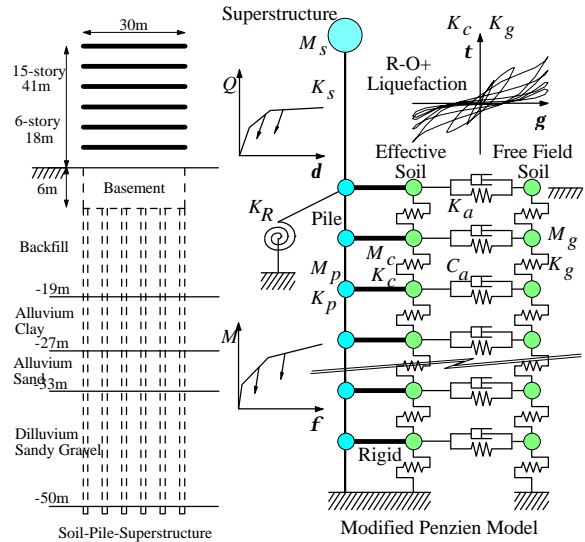


Fig. 9 A Pile-Supported Structure and its Penzien Model

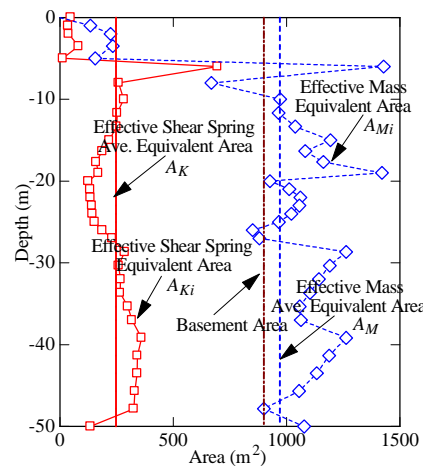


Fig. 10 Equivalent Area for Modified Penzien Model

Table 2 Analysis Cases

Pile	Soil	R-O Nonlinear	Liquefied
	Linear		CASE 1
Nonlinear		CASE 3	CASE 4

Figs. 13 and 14 show the maximum bending moments and shear forces of a pile. The moment distribution varies upper through lower clay layer(G.L. -19m ~ -27m) in each analysis cases. The bending moment of upper layer than G.L. -19m indicates the following relation CASE 2 > CASE 1 > CASE 4 > CASE 3 i.e. the soil liquefaction makes moment large and pile nonlinearity make moment small.

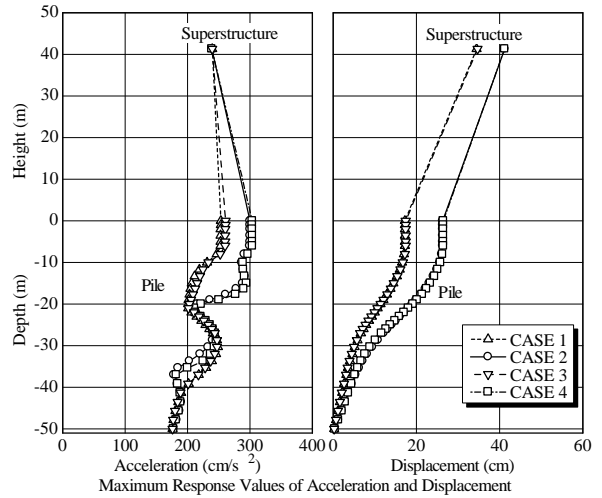
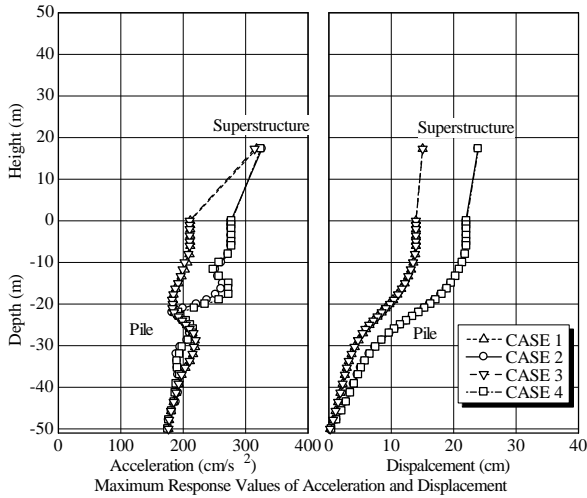
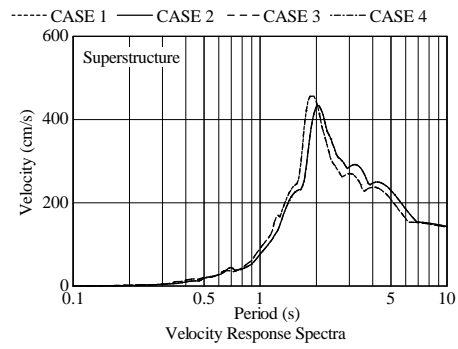
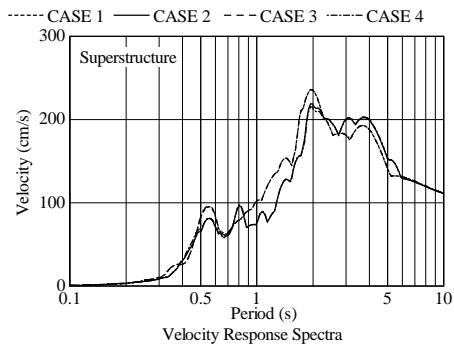
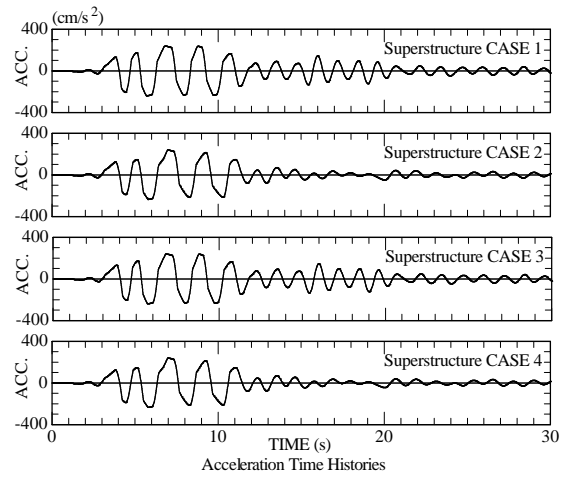
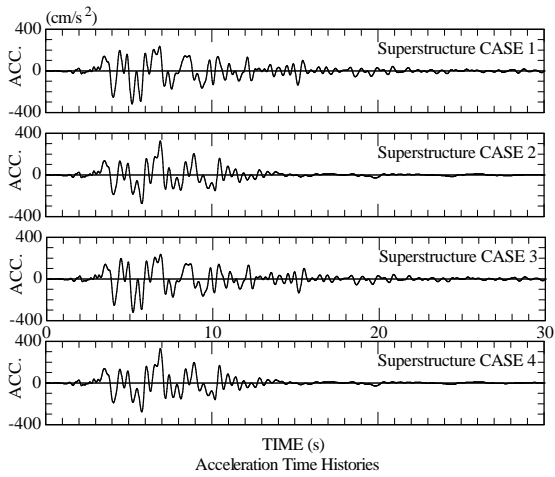


Fig. 11 Responses of 6 Story Structure

Fig. 12 Responses of 15 Story Structure

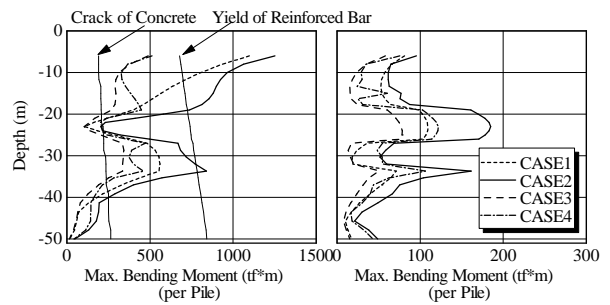
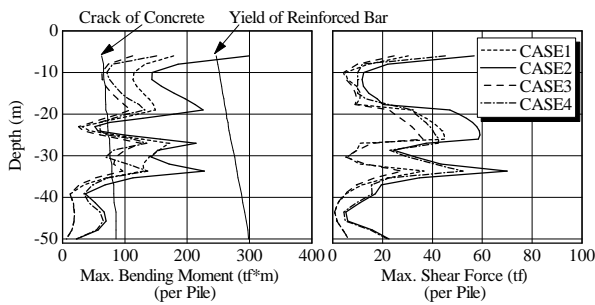


Fig. 13 Responses of Piles that support 6 Story Structure

Fig. 14 Responses of Piles that support 15 Story Structure

The soil liquefaction influences on the bending moment of G.L. -27m ~ -40m layer.

The effect of pile nonlinearity is small for the shear force of lower G.L. -33m layer as same as the tendency of the acceleration.

Comparing 6 and 15 stories models, the distribution of maximum values of bending moment and shear force in pile are similar. 15 stories model shows that the pile at all depth occurs large moment. The pile nonlinearity suppresses the bending moment when progresses the deformation beyond the crack of concrete.

4. Concluding remarks

This paper proposed an analytical technique by which liquefaction can be considered and the validity was verified by the simulation analysis of the observed records of Kobe Port Island. A proposed technique can easily evaluate the liquefaction characteristic using parameters based on SPT-N value even when there is no detailed laboratory examination. It is found that the free field responses show the nonlinear features : i.e. very small amplitude of acceleration and the inverse S shaped stress-strain relationship, and the change of the acceleration is steep in the vicinity of the layer boundary of the clay layer and backfill soil. The bending moments of pile become large as to soil liquefaction, and small as to nonlinearity of pile. The distribution of the maximum response value is greatly different according to the soil liquefied or not where geological features change between sand layer and clay layer. However, the liquefaction and pile nonlinearity has little influence over the response of the superstructure.

The followings should be considered in the future.

(1) Relationship between nonlinearity of soil and effect of pile groups

The interaction soil spring and effect of pile groups are accurately determined according to three dimensional thin layer element method used in this

paper. However, the effects of pile groups are uncertain when the nonlinearity of soil become large.

(2) Axial force - moment - curvature relation of pile

The inertial force from the superstructure makes the axial force fluctuate in the pile at the edge of foundation, and it causes to decrease the pile strength. Moreover, it is important to confirm the validity of an analytical technique using observation records.

References

Architectural Institute of Japan : Recommendations for design of building foundations (in Japanese), 430p., 1988

Fujimori et al. : Non-linear seismic response analytical method for pile group foundation building considering frequency characteristics of impedance (in Japanese), Reports of Technical Research Institute, No.56, pp. 9-14, 1998

Ishihara, K. et al. : One-dimensional soil response analysis during earthquakes based on effective stress method , Journal of the faculty of engineering ,University of Tokyo ,Vol.35 ,No.4 , pp.656-699 , (1980)

Kobe City Development Beareau : Report on soil exploration and earthquake observation of Kobe Port Island (in Japanese), 1995

Miyamoto et al. : Response of pile foundation in liquefied soil deposit during the Hyogo-ken Nanbu earthquake of 1995 (in Japanese), J. Struct. Constr. Eng., AIJ, No. 493, pp. 23-30, 1997

Seed, H. B. et al., Pore-pressure changes during soil liquefaction, ASCE, Vol. 102, GT4, pp. 323-346, 1976

Shamoto et al. : Applicability of a one-dimensional effective stress analysis to an existing soil deposit (in Japanese), J. Struct. Constr. Eng., AIJ, No. 433, pp. 113-119, 1992

Takano et al. : Dynamic response analysis of embedded foundation on pile groups (in Japanese), Proc. JEES, Vol. 1, pp. 1195-1120, 1994